proceedings

MDPI

Proceedings

Ionospheric Effects of Natural Hazards in Geophysics: From Single Examples to Statistical Studies Applied to M5.5+ Earthquakes†

Dedalo Marchetti [1], Kaiguang Zhu [1], Rui Yan [2], Zeren Zhima [2], Shen Xuhui [2], Wenqi Chen [1], Yuqi Cheng [1], Mengxuan Fan [1], Ting Wang [1], Jiami Wen [1], Donghua Zhang [1], Hanshuo Zhang [1] and Yiqun Zhang [1]

[1] College of Instrumentation and Electrical Engineering, Jilin University, Changchun 130061, China; dedalomarchetti@jlu.edu.cn (D.M.); zhukaiguang@jlu.edu.cn (K.Z.);
[3] Space Observation Research Center, National Institute of Natural Hazards, MEMC, Beijing 100085, China; ruiyan@ninhm.ac.cn (R.Y.); zerenzhima@ninhm.ac.cn (Z.Z.); xuhuishen@ninhm.ac.cn (X.S.);
† Presented at "The 4th International Electronic Conference on Geosciences (online)".

Abstract: Geophysical natural hazards, such as earthquakes and volcano eruptions, can have catastrophic effects on the population depending on the location and quality of construction. From the geophysical point of view, several aspects are still debated in the preparation phase of such events. In particular, several theories proposed that prior to the earthquake and volcano eruption, the releases of gas, fluids or charged particle from the lithosphere (e.g., the fault for the earthquake) could create some effects on the atmosphere and ionosphere. In this work, several single examples will be shown of possible candidates of pre-earthquake ionospheric disturbances recorded by the China National Space Administration (in partnership with the Italian Space Agency) China Seismo Electromagnetic Satellite (CSES) or European Space Agency *Swarm* constellation. The examples will show anomalous ionospheric status in terms of magnetic disturbances or increase of electron density before earthquakes like Mw = 7.1 Ridgecrest (US) 2019 or during the large recent volcano eruption of Hunga Tonga-Hunga Ha'Apai of last 15 January 2022. In these cases, some couplings between the lithosphere and ionosphere are proposed. Finally, verifying if such ionospheric disturbances proceeded for "chance" or are really linked to the incoming event is a crucial point. For this purpose, we performed worldwide statistical studies, not only supporting the recurrence of such phenomena for about 15% of M5.5+ shallow earthquakes but also showing a link between the magnitude of the upcoming seismic events and the pre-earthquake anticipation time. Furthermore, we also show the influence of the location (sea or land) on the frequency of the ionospheric electromagnetic disturbance.

Keywords: ionosphere; earthquake; precursors; LAIC; CSES; Swarm

Citation: Marchetti, D.; Zhu, K.; Yan, R.; Zhima, Z.; Xuhui, S.; Chen, W.; Cheng, Y.; Fan, M.; Wang, T.; Wen, J.; et al. Ionospheric Effects of Natural Hazards in Geophysics: From Single Examples to Statistical Studies Applied to M5.5+ EarthQuakes. **2022**, *69*, x. https://doi.org/10.3390/xxxxx

Academic Editor(s):

Received: date
Accepted: date
Published: date

1. Introduction

The existence of ionospheric pre-earthquake electromagnetic disturbances is a controversial topic among researchers. Despite the scepticism of some researchers several pieces of evidence exist of such disturbances. In particular, several single earthquake studies provide empirical evidence for ionospheric anomalies before large earthquakes in the World; for example, Mansouri et al. [1] showed perturbations before M8.3 Chile 2015 earthquake. In addition, statistical studies, particularly on the DEMETER satellite that flew from 2004 to 2010, provided proof that shallow M4.8+ earthquakes were statistically preceded by electron density anomalies in the 15 days before the earthquakes [2,3]. Several Lithosphere, Atmosphere, and Ionosphere Coupling (LAIC) models support pre-earthquake ionospheric disturbances. Unfortunately, there is no unique LAIC model. At the present state of the art, it is unclear if the various models describe more coupling ways

or if some of them are wrong. They are based on a chain of phenomena that started with the air ionisation induced by radon released from the fault (e.g., Pulinets and Ouzounov [4]) or generation of positive holes (p-holes) as suggested by Freund [5] or a direct electromagnetic ULF emission from the micro-crack by Molchanov and Hayakawa [6] or even Acoustic Gravity Wave induced by thermal heating of Earth surface [7].

This short paper will present a few examples of ionospheric pre-earthquakes and volcano ionospheric disturbances and, finally, a systematical statistical investigation of China Seismo Electromagnetic Satellite (CSES) electron density and M5.5+ earthquakes still supporting the existence of such pre-earthquake phenomena.

All the earthquake analyses have been performed inside a circular area that scales exponentially with the moment magnitude as defined by Dobrovoslky et al. [8].

2. Results

Here we present some examples of anomalies before two earthquakes: Mw = 8.3 Chile 2015 and Mw = 7.1 Ridgecrest (US) 2019 and during and after the large Volcanic Explosive Index (VEI) = 6 Hunga Tonga-Hunga Ha'apai eruption of last 15 January 2022.

3.1. Mw = 8.3 Illapel (Chile) 16 September 2015 Earthquake

On 16 September 2015 at 22:54:32 UT, a large earthquake of moment magnitude Mw = 8.3 hit Chile close to Illapel, with its epicentre localised at 31.573°S, 71.674°W. Until now, this is the largest earthquake that occurred during the ESA Swarm mission. De Santis et al. [9] studied the Swarm magnetic and electron density data one month before and after the earthquake, together with 11 other seismic events with a magnitude of 6.1 or greater. The most interesting result of that paper is the correlation between the number of detected magnetic or electron density anomalies and earthquake magnitude. Despite this, such a study was limited to only one month before the earthquake. At the same time, several other investigations provide evidence for anomalies even before, particularly large earthquakes [10–12]. For this purpose, in Figure 1 and Figure 2, we show an example of an anomaly in the magnetic field, especially in the Y-East component that appeared about 258 days before the mainshock, very close to the future epicentre. Such anomaly has its magnetic conjugate with a bit lower intensity and shorter, supporting the hypothesis that the anomaly's source was above the epicentre and it propagated in the conjugated point following geomagnetic field lines, losing part of the energy as predicted by the theories [13]. Looking at the following tracks, we still notice the presence of the anomaly in the Y-East component in track 11 fully inside Dobrosvolsky's area and still close to the future epicentre (little shifted northward according to the magnetic field direction). Contrariwise, even though we detected a clear anomaly outside the Dobrovolsky in track 13 (green line in Figure 2), its shape is totally different. In fact, it presents a larger intensity far from the centre of the anomaly, like a butterfly shape, so we think this is likely another source compared to the phenomenon depicted in Track 9 and 11 inside the Dobrovolsky.

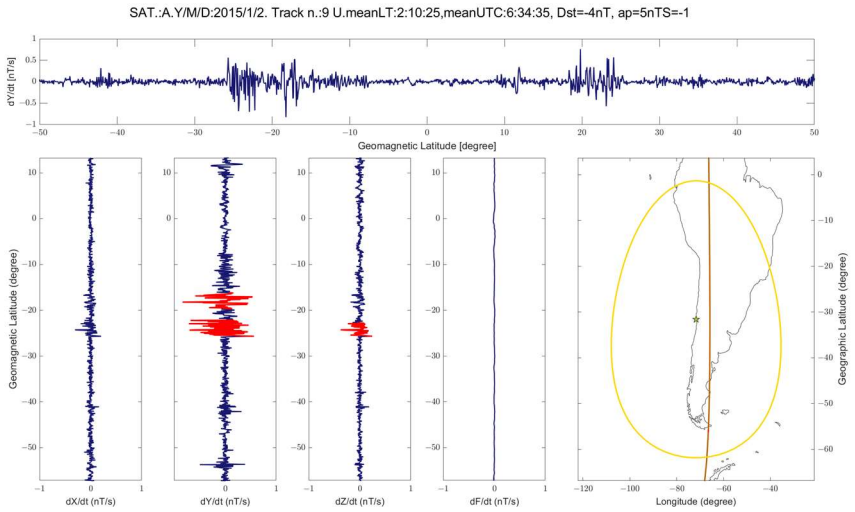

Figure 1. Swarm Alpha magnetic field residual, track 9 on 2 January 2015, i.e., 258 days before M8.3 Illapel (Chile) 2015 earthquake. The 3° latitude anomalous (k_t = 2.5) windows are marked by red colour. The map of the region is represented with a yellow circle that shows the Dobrovolsky area of the earthquake, whose epicentre is marked with a green star and the satellite track projection by a brown line. The title indicates which satellite is represented (A = Alpha, B = Bravo, C = Charlie), the date of acquisition, track number, the direction of fly (U = Upward, D = Downward), local time (meanLT) and universal time (meanUT) at the middle of the plotted track. Geomagnetic indexes Dst and ap at acquisition time as also reported.

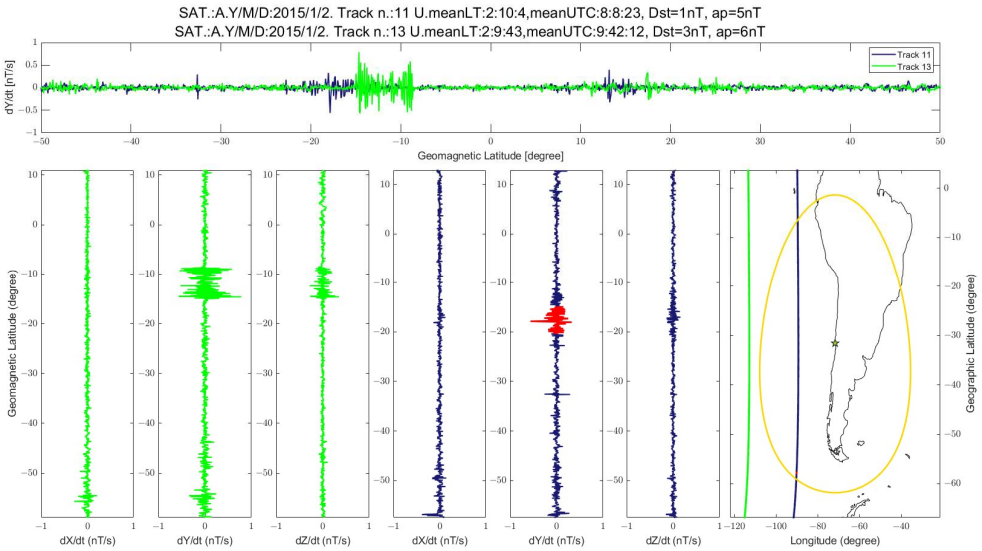

Figure 2. Tracks 11 (blue colour) and track 13 (green colour), following the one in Figure 1. As in Figure 1, the anomalies are marked by red lines, and the representation and the title information are the same of Figure 1. Track 13 has no "red" anomaly as it's outside Dobrovolsky's area and the code automatically excludes it.

3.2. Mw = 7.1 Ridgecrest (California, US) 6 July 2019 Earthquake

On 6 July 2019 at 3:19:53 UT, an earthquake of moment magnitude 7.1 was localised close to Ridgecrest in California (US). It was a result of the strike-slip focal mechanism, and its depth was estimated at ~8.0 km. De Santis et al. [14] claimed a chain of processes compatible with a LAIC and characteristics of complex systems, like earthquakes. Furthermore, an increase of magnetic anomalies was detected by Swarm satellites about 220 days before the earthquake by Marchetti et al. [15] and anomalies in Total Electron Content and CSES-01 Ne data about one week before the mainshock by Xie et al. [16]. In addition, De Santis et al. [14] identified an increase of electron density 33 days prior to the

mainshock as unique in several months of data investigation from Point Arguello ionosonde (whose position is represented by the blue triangle in the map in Figure 3) and Swarm Alpha here reported in Figure 3. We also checked the electron density recorded by CSES-01 on the same night at a very short time difference (just 13 minutes before). The CSES satellite didn't record any anomalous electron density value.

This apparent discrepancy can be described in two different ways. The first one is that the increase of electron density occurred only westward to the future epicentre. The second explanation could be that such an electron density increase, supposed to come from the internal layer (the lithosphere), did not reach the higher altitude of the CSES satellite (about 510 km) compared with the one of Swarm Alpha at that time (about 470 km). We tend to exclude that the ionosphere could have changed in a much shorter time.

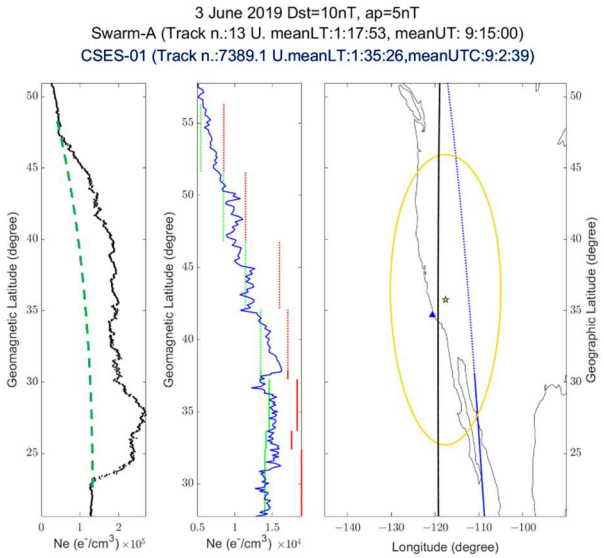

Figure 3. Increase of electron density about one month before Mw = 7.1 Ridgecrest (California, US) 6 July 2019 earthquake. Electron Density (Ne) data are from Swarm Alpha (black) and CSES-01 (blue) satellites. The map and the title information are the same of Figure 1.

3.3. Hunga Tonga-Hunga Ha'apai Volcano Explosion Effect in the Ionosphere

On 15 January 2022, the submarine stratovolcano Hunga Tonga-Hunga Ha'Apai produced a wide explosion estimated with a Volcano Explosive Index (VEI) of about 6 [17]. Several researchers are investigating such a large and rare geophysical event, considering that it's the first time it is possible to monitor and observe such a geophysical event from several satellites [18–20]. Here we further investigate the CSES satellite electron density measurements already presented by D'Arcangelo et al. [21]. During the volcano explosion (estimated from seismic data at 4:15:45 UTC), CSES-01 was flying westward of the volcano (see Figure 4). In order to search if the electron density profile could contain some signature of the volcano explosion, we compared the Ne profile with the one of the previous track at the same local time (about 2:00 PM).

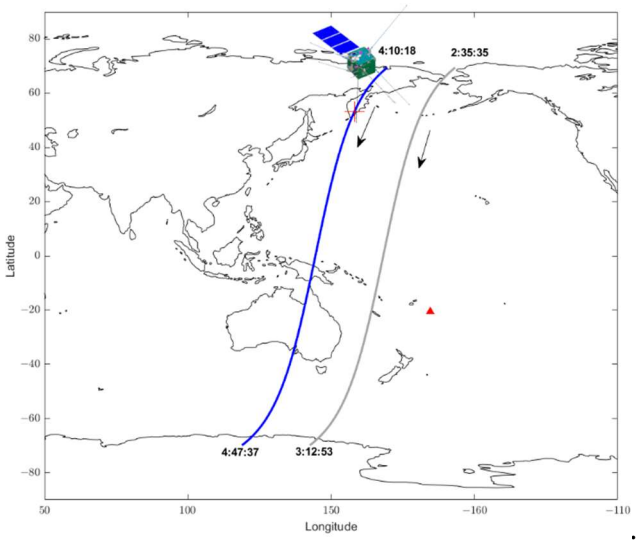

Figure 4 Map with start and end UT times of CSES-01 satellite in the track before (grey) and during (blue) the explosion of Hunga Tonga-Hunga Ha'apai volcano represented as a red triangle. The satellite's position at the time of the explosion is marked with a red cross. Both tracks are in descending (daytime) directions as indicated by the black arrows.

In particular, in Figure 5, we have decomposed the electron density latitudinal profiles in 5 different frequency bands from the continuum (DC) to half of the sampling frequency of 333 mHz. As the two orbits were descending, the time went from right to left. So, the blue data at the left of the red vertical line (time of the explosion) are acquired after it, the blue on the right, and all the grey before it. In particular, we noted an increment of electron density and some slow oscillations (underlined by red oval) that are unique in the track after the explosion from about 44°N to 32°N, as visible in subpanels d and e of Figure 5. In the previous paper, this disturbance was underlined with a red circle and the number "1" in Figure 15 of [21]. We propose that such disturbance is the ionospheric shock induced by the explosion by electromagnetic coupling between the atmosphere/ocean (i.e., under the sea where the explosion originated) and the ionosphere. It can be explainable only by electromagnetic mechanism due to the very short time and the relatively far position of the satellite at the time of the explosion (overflying the Kamchatka Islands, see Figure 4).

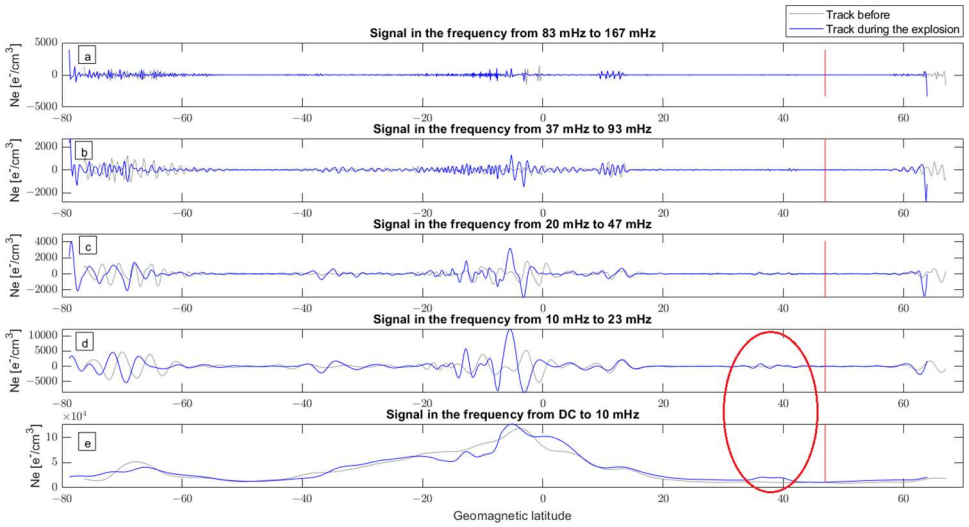

Figure 5. Frequency investigation of the electron density profile of CSES acquired during the Hunga Tonga Hunga Ha'Apai volcano eruption of 15 January 2022 at 4:15:45 UTC. The blue and grey lines

represent the signal acquired in the daytime orbits during and before the explosion, respectively. The signal has been decomposed into 5 frequency bands: (a) from 83 mHz to 167 mHz; (b) from 37 mHz to 93 mHz; (c) from 20 mHz to 47 mHz; (d) from 10 mHz to 23 mHz; (e) from DC to 10 mHz; The vertical red line represents the position of the CSES satellite at the eruption time. Both tracks are descending.

Such a violent volcano explosion generated a pressure wave (Lamb wave) that propagated at the sound speed all around the Earth and was globally recorded by barometric sensors [21–23]. In particular CSES-01 satellite orbit at around 10 UT passed almost tangent to the Lamb wavefront (see Figure 17 in [21]), and we provided further details of this orbit in Figure 6. We calculated a smoothed signal by a moving average window of 11 samples to remove possible oscillation of the measurements that is unclear whether they are due to the instrument or a real oscillation of the ionosphere. The distance of the satellite with respect to the front of the pressure wave has also been calculated, taking into account that both the satellite and the front wave are moving simultaneously. The pressure wave has been simplified as perfectly circular, and its speed has been considered fixed at 1100 km/hour. Actually, the speed depends on air temperature and can be influenced by orography, but our calculus could be a first approximation. Finally, we calculate the correlation between the smoothed electron density and the surface atmospheric pressure provided by ECMWF ERA-5 [24]. The correlation between the two profiles is 36%, supporting the coupling between the atmosphere and the ionosphere. Even though the ionosphere electron density seems reasonably correlated (considering the distance of the geo-layers), only a part of the track could be affected by the Lamb wave that, in any case, seems to have perturbed the electron density in the ionosphere.

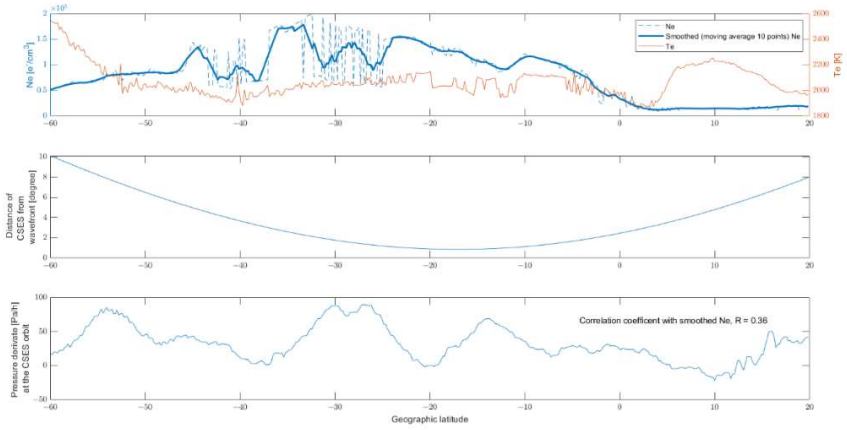

Figure 6. Detailed investigation of the electron density profile of CSES-01 satellite probably affected by the ionospheric effect of Lamb wave produced by the Hunga Tonga-Hunga Ha'apai volcano explosion of 15 January 2022.

3.3. Worldwide Statistical Investigation of Ionospheric Electron Density Measured by CSES-01

A limitation of single case studies, as in the previous examples, is that some anomalies could appear before the geophysical hazard just for a chance but are not related to the incoming event. To address this problem, a statistical study on many events, such as the M5.5+ Worldwide earthquakes, can prove (or not) the relationship between ionospheric anomalies and earthquakes. De Santis et al. [11] and Marchetti et al. [12] provided strong evidence that not only a consistent number of M5.5+ shallow earthquakes are proceeded by Swarm magnetic and electron density anomalies but also that the anticipation time increase with the magnitude according to the Rikitake's law [10] and that the frequency of magnetic anomaly seems to depend on sea or land epicentre location. De Santis et al. [25] conducted a preliminary analysis of CSES Ne anomalies related to M5.5+ earthquakes that we extended to 24 months of data (i.e., two years).

Figure 7 shows the result of the Worldwide Statistical Correlation (WSC) algorithm (details of the methods in [11,12]) applied to CSES electron density data. The 5.5+ earthquakes were investigated in a symmetric period of 90 days before until 90 days after the 568 seismic events. We immediately note that the results present interesting features and are statistically significant. The analysis shows more pre-earthquake than post-earthquake anomalies. In addition, the absolute maximum concentration is located before the earthquakes. Despite a large number of total extracted anomalies (169840), the statistical significance of the concentrations potentially related to the pre-earthquake process is relatively high (i.e., 1.8 higher than a random concentration as indicated by the "d" factor defined in [11,12]). Furthermore, it's outstanding that a significantly higher number of anomalies (6654) were located in the 90 days before the earthquakes compared to the lower number of anomalies (5928) in the 90 days following the same events. Finally, it seems that from about 56 days before the earthquake, there is an activation of the ionosphere showing a "swarm" of anomalies with a peak of about one month before the earthquake origin time. Future studies are necessary to further extend the analysis at 4.5 years (or more) of CSES mission data and investigate deeply the relationship between CSES anomalies and earthquakes with a similar approach already used for Swarm in [11,12].

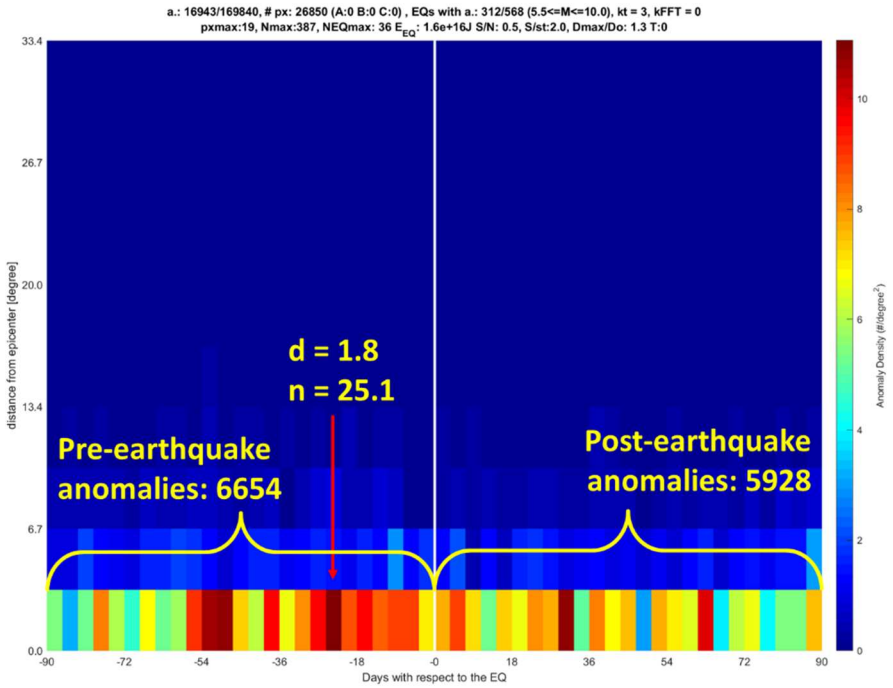

Figure 7. WSC algorithm applied to CSES Ne anomalies (recorded in April, August and September 2018, in 2019 and from January to September 2020) correlated with M5.5+ earthquakes from 90 days before until 90 days after the event. The number of anomalies in the first row before and after the earthquakes is also reported. Two statistical parameters for the maximum anomaly concentration, "d" and "n", are reported. "d" represent how many time the concentration is higher than the average random one and n how many standard deviations of random simulation such concentration is higher (full definition and details in [11,12]).

3. Discussion and Conclusions

The study of ionospheric disturbances is often afforded by investigating a geophysical hazard event or by a statistical approach to a wide number of case studies. Both methodologies present pro and contra. The former permits us to deeply investigate what happened before the specific event taking into account several factors, from the geomagnetic conditions to the tectonic and geological settings, while it isn't able to distinguish if some alterations of the ionosphere are by chance or really related to the incoming event. A statical study like the one we show in Figure 7 allows us to confirm whether a phenomenon

is recurrent or not, but it lacks specific details. For example, we show evidence that about 20 days before 36 earthquakes, there is a significant concentration of CSES Ne anomalies 1.8 times higher than what was expected by chance. Still, the details, such as, which LAIC mechanisms, if there is or not the conjugate anomaly (as in the example shown in **Figure 1**) are missing. Finally, even if we confirm the existence of LAIC prior to earthquakes, future studies need to understand better the LAIC propagation mechanisms and the features that influence the LAIC ways.

Author Contributions: Conceptualisation, methodology, software, formal analysis, investigation, visualisation, writing—original draft preparation, D.M.; validation, supervision, project administration, funding acquisition, K.Z. and D.M, data curation, D.M and Y.R.; writing—review and editing, all authors.. All authors have read and agreed to the published version of the manuscript.

Funding: This research was funded by the National Natural Science Foundation of China, grant number 41974084; the China Postdoctoral Science Foundation, grant number 2021M691190; the International Cooperation Project of the Department of Science and Technology of Jilin Province, grant number 20200801036GH.

Institutional Review Board Statement and Informed Consent Statement: Not applicable.

Data Availability Statement: *Swarm* data are freely available via ftp and http at swarm-diss.eo.esa.int server (last access on 27 July 2022). China Seismo Electromagnetic Satellite data are freely available at www.leos.ac.cn (last access on 15 December 2020) upon registration and approval.

Acknowledgments: We acknowledge Saioa Arquero Campuzano, Dario Sabbagh, Martina Orlando, Loredana Perrone, Rita Di Giovambattista, Giorgiana De Franceschi, Maurizio Soldani, Domenico Di Mauro, Adriano Nardi, Cristiano Fidani, Salvatore Roberto Maugeri, Alessandro Bonforte, Mauro Regi, Angelo De Santis, Serena D'Arcangelo, Gianfranco Cianchini, Alessandro Ippolito, to have participated in some scientific discussions of the present work.

Conflicts of Interest: The authors declare no conflict of interest. The funders had no role in the design of the study; in the collection, analyses, or interpretation of data; in the writing of the manuscript, or in the decision to publish the results.

References

1. Mansouri Daneshvar, M.R.; Freund, F.T. Remote Sensing of Atmospheric and Ionospheric Signals Prior to the Mw 8.3 Illapel Earthquake, Chile 2015. *Pure Appl. Geophys.* **2017**, *174*, 11–45, doi:10.1007/s00024-016-1366-0.
2. Michel Parrot Statistical Analysis of Automatically Detected Ion Density Variations Recorded by DEMETER and Their Relation to Seismic Activity. *Annals of Geophysics* **2012**, *55*, doi:10.4401/ag-5270.
3. Yan, R.; Parrot, M.; Pinçon, J.-L. Statistical Study on Variations of the Ionospheric Ion Density Observed by DEMETER and Related to Seismic Activities: Ionospheric Density and Seismic Activity. *J. Geophys. Res. Space Physics* **2017**, *122*, 12,421-12,429, doi:10.1002/2017JA024623.
4. Pulinets, S.; Ouzounov, D. Lithosphere–Atmosphere–Ionosphere Coupling (LAIC) Model – An Unified Concept for Earthquake Precursors Validation. *Journal of Asian Earth Sciences* **2011**, *41*, 371–382, doi:10.1016/j.jseaes.2010.03.005.
5. Freund, F. Pre-Earthquake Signals: Underlying Physical Processes. *Journal of Asian Earth Sciences* **2011**, *41*, 383–400, doi:10.1016/j.jseaes.2010.03.009.
6. Molchanov, O.A.; Hayakawa, M. Generation of ULF Electromagnetic Emissions by Microfracturing. *Geophys. Res. Lett.* **1995**, *22*, 3091–3094, doi:10.1029/95GL00781.
7. Hayakawa, M.; Kasahara, Y.; Nakamura, T.; Hobara, Y.; Rozhnoi, A.; Solovieva, M.; Molchanov, O.; Korepanov, V. Atmospheric Gravity Waves as a Possible Candidate for Seismo-Ionospheric Perturbations. *JAE* **2011**, *31*, 129–140, doi:10.1541/jae.31.129.
8. Dobrovolsky, I.P.; Zubkov, S.I.; Miachkin, V.I. Estimation of the Size of Earthquake Preparation Zones. *PAGEOPH* **1979**, *117*, 1025–1044, doi:10.1007/BF00876083.
9. De Santis, A.; Marchetti, D.; Spogli, L.; Cianchini, G.; Pavón-Carrasco, F.J.; Franceschi, G.D.; Di Giovambattista, R.; Perrone, L.; Qamili, E.; Cesaroni, C.; et al. Magnetic Field and Electron Density Data Analysis from Swarm Satellites Searching for Ionospheric Effects by Great Earthquakes: 12 Case Studies from 2014 to 2016. *Atmosphere* **2019**, *10*, 371, doi:10.3390/atmos10070371.
10. Rikitake, T. Earthquake Precursors in Japan: Precursor Time and Detectability. 18.
11. De Santis, A.; Marchetti, D.; Pavón-Carrasco, F.J.; Cianchini, G.; Perrone, L.; Abbattista, C.; Alfonsi, L.; Amoruso, L.; Campuzano, S.A.; Carbone, M.; et al. Precursory Worldwide Signatures of Earthquake Occurrences on Swarm Satellite Data. *Sci Rep* **2019**, *9*, 20287, doi:10.1038/s41598-019-56599-1.

12. Marchetti, D.; De Santis, A.; Campuzano, S.A.; Zhu, K.; Soldani, M.; D'Arcangelo, S.; Orlando, M.; Wang, T.; Cianchini, G.; Di Mauro, D.; et al. Worldwide Statistical Correlation of Eight Years of Swarm Satellite Data with M5.5+ Earthquakes: New Hints about the Preseismic Phenomena from Space. *Remote Sensing* **2022**, *14*, 2649, doi:10.3390/rs14112649.
13. Liperovsky, V.A.; Pokhotelov, O.A.; Meister, C.-V.; Liperovskaya, E.V. Physical Models of Coupling in the Lithosphere-Atmosphere-Ionosphere System before Earthquakes. *Geomagn. Aeron.* **2008**, *48*, 795–806, doi:10.1134/S0016793208060133.
14. De Santis, A.; Cianchini, G.; Marchetti, D.; Piscini, A.; Sabbagh, D.; Perrone, L.; Campuzano, S.A.; Inan, S. A Multiparametric Approach to Study the Preparation Phase of the 2019 M7.1 Ridgecrest (California, United States) Earthquake. *Front. Earth Sci.* **2020**, *8*, 540398, doi:10.3389/feart.2020.540398.
15. Marchetti, D.; De Santis, A.; Campuzano, S.A.; Soldani, M.; Piscini, A.; Sabbagh, D.; Cianchini, G.; Perrone, L.; Orlando, M. Swarm Satellite Magnetic Field Data Analysis Prior to 2019 Mw = 7.1 Ridgecrest (California, USA) Earthquake. *Geosciences* **2020**, *10*, 502, doi:10.3390/geosciences10120502.
16. Xie, T.; Chen, B.; Wu, L.; Dai, W.; Kuang, C.; Miao, Z. Detecting Seismo-Ionospheric Anomalies Possibly Associated With the 2019 Ridgecrest (California) Earthquakes by GNSS, CSES, and Swarm Observations. *JGR Space Physics* **2021**, *126*, doi:10.1029/2020JA028761.
17. Poli, P.; Shapiro, N.M. Rapid Characterization of Large Volcanic Eruptions: Measuring the Impulse of the Hunga Tonga Ha'apai Explosion From Teleseismic Waves. *Geophysical Research Letters* **2022**, *49*, doi:10.1029/2022GL098123.
18. Heki, K. *Ionospheric Signatures of Repeated Passages of Atmospheric Waves by the 2022 Jan. 15 Hunga Tonga Eruption Detected by QZSS-TEC Observations in Japan*; In Review, 2022;
19. Matoza, R.S.; Fee, D.; Assink, J.D.; Iezzi, A.M.; Green, D.N.; Kim, K.; Toney, L.; Lecocq, T.; Krishnamoorthy, S.; Lalande, J.-M.; et al. Atmospheric Waves and Global Seismoacoustic Observations of the January 2022 Hunga Eruption, Tonga. *Science* **2022**, *377*, 95–100, doi:10.1126/science.abo7063.
20. Yuen, D.A.; Scruggs, M.A.; Spera, F.J.; Zheng, Y.; Hu, H.; McNutt, S.R.; Thompson, G.; Mandli, K.; Keller, B.R.; Wei, S.S.; et al. Under the Surface: Pressure-Induced Planetary-Scale Waves, Volcanic Lightning, and Gaseous Clouds Caused by the Submarine Eruption of Hunga Tonga-Hunga Ha'apai Volcano. *Earthquake Research Advances* **2022**, 100134, doi:10.1016/j.eqrea.2022.100134.
21. D'Arcangelo, S.; Bonforte, A.; De Santis, A.; Maugeri, S.R.; Perrone, L.; Soldani, M.; Arena, G.; Brogi, F.; Calcara, M.; Campuzano, S.A.; et al. A Multi-Parametric and Multi-Layer Study to Investigate the Largest 2022 Hunga Tonga–Hunga Ha'apai Eruptions. *Remote Sensing* **2022**, *14*, doi:10.3390/rs14153649.
22. Amores, A.; Monserrat, S.; Marcos, M.; Argüeso, D.; Villalonga, J.; Jordà, G.; Gomis, D. Numerical Simulation of Atmospheric Lamb Waves Generated by the 2022 Hunga-Tonga Volcanic Eruption. *Geophysical Research Letters* **2022**, *49*, doi:10.1029/2022GL098240.
23. Lin, J.; Rajesh, P.K.; Lin, C.C.H.; Chou, M.; Liu, J.; Yue, J.; Hsiao, T.; Tsai, H.; Chao, H.; Kung, M. Rapid Conjugate Appearance of the Giant Ionospheric Lamb Wave Signatures in the Northern Hemisphere After Hunga-Tonga Volcano Eruptions. *Geophysical Research Letters* **2022**, *49*, doi:10.1029/2022GL098222.
24. Hersbach, H.; Bell, B.; Berrisford, P.; Hirahara, S.; Horányi, A.; Muñoz-Sabater, J.; Nicolas, J.; Peubey, C.; Radu, R.; Schepers, D.; et al. The ERA5 Global Reanalysis. *Q.J.R. Meteorol. Soc.* **2020**, *146*, 1999–2049, doi:10.1002/qj.3803.
25. Statistical Correlation Analysis of Strong Earthquakes and Ionospheric Electron Density Anomalies as Observed by CSES-01. *Il Nuovo Cimento C* **2021**, *44*, 1–4, doi:10.1393/ncc/i2021-21119-1.